Electrochemical studies on Li^+/K^+ ion exchange behaviour in $K_4Fe(CN)_6$ cathode material for Li, K-ion battery

BIKASH MANDAL[b], I BASUMALLICK[b] and SUSANTA GHOSH[a,*]

[a]Electrochemistry Laboratory, Integrated Science Education and Research Centre, Visva-Bharati University, Santiniketan 731235, India

[b]Electrochemistry Laboratory, Department of Chemistry, Visva-Bharati University, Santiniketan 731 235, India

e-mail: susanta.ghosh@visva-bharati.ac.in

Abstract. The electrochemical studies of anhydrous $K_4Fe(CN)_6$ is reported. Anhydrous material was produced after dehydrating $K_4Fe(CN)_6.3H_2O$ crystal at 200°C in an open atmosphere. The material, as obtained, was characterized by various spectroscopic techniques, such as UV-Visible, FTIR, powder X-ray diffraction and FESEM-EDX. Electrochemical and Li^+/K^+ ion exchange behaviour of the synthesized material were studied by cyclic voltametry (CV), chronoamperometry (CA) and galvanostatic charge-discharge method after preparing a laboratory model cell against lithium anode instead of potassium. During anodic scan in the 1st cycle, peak maximum was observed at 3.93 V vs. Li^+/Li due to removal of K^+ ions from the ferrocyanide matrix, whereas, in the reverse scan (cathodic sweep) as well as in consequent cycles, peak maxima due to Li^+ ion insertion and extraction were observed at 2.46 V and 3.23 V vs. Li^+/Li, respectively. Cell, assembled using ferrocyanide cathode and lithium anode, shows an open circuit potential of 3.08 V and delivers a maximum capacity of 61 mAh g^{-1} (theoretical capacity 72 mAh g^{-1}) at a rate of 0.2 C at room temperature.

Keywords. $K_4Fe(CN)_6$ cathode material; powder XRD; cyclic voltametry; charge-discharge; Li, K-ion battery.

1. Introduction

Demand for lithium-ion batteries is increasing by the day.[1] They are widely used in portable electronic devices. There are several reasons for its popularity such as large energy-to-weight ratio, absence of memory effect, and low energy fading during rest.[2,3] Beyond consumer electronics, lithium-ion batteries are used in applications in defence, electric vehicles and aerospace, because it has the greatest electrochemical potential and provide the highest energy density, 125–150 Whk g^{-1}.[4]

LiCoO$_2$ is used as the cathode material in commercial lithium-ion batteries, but its component element, cobalt is very expensive and toxic, which limits its application in large scale. Therefore, new low cost cathode material is required. In the last few years, a number of new cathode materials were proposed.[2,3] However, none of them are found suitable for commercial applications due to different critical issues, such as toxicity, higher resistivity, smaller specific capacity, low operating potential, lower cyclability, lower rate capability, etc.[5–7] Among them, layered structure of LiMnO$_2$[8–11] and spinel LiMn$_2$O$_4$[12–14] compounds have drawn more

attention, irrespective of their low lithium-ion diffusion coefficient and large capacity fading upon cycling.

Recently,[15] lithium iron phosphate (LiFePO$_4$) became an attractive alternating cathode material, due to some advantages *viz.* low cost and environment friendly starting materials,[5–7] excellent cycling performance, high theoretical capacity (170 mAh g^{-1}), high safety, good operating voltage and high temperature performance.[16–20] The main demerit associated with this material is its lower electronic conductivity that results in lower diffusion coefficient of lithium ions and consequently, poor rate capability. Some efforts to increase its conductivity have been made after doping with higher valence metal cations, like Ti^{4+}, Ga^{3+}, Zr^{4+}, W^{6+}, V^{3+}, etc.[21–23] and thus few fold enhancements in conductivity was found. Its performance was further improved by synthesizing nano size particles using different particle size-controlled techniques like solution–based,[24] sol-gel,[17–21] and solid-state[16] methods. There are a few reports available on the synthesis of nano LiFePO$_4$[17,20,21] over large surface area of carbon powder with better performance and cyclability.

Among all the synthesis methodologies reported for LiFePO$_4$, one factor that is common is the inert atmosphere at high temperature in order to prevent oxidation of Fe^{2+} to Fe^{3+}.[23,24] Use of ultra-high pure N$_2$

*For correspondence

or Ar along with required instrumentation makes the synthesis of LiFePO$_4$ as expensive and difficult process.

In this paper, we report an environment friendly K$_4$Fe(CN)$_6$[25,26] as cathode material for rechargeable Li, K-ion battery.[27–29] It was synthesized by just dehydrating its hydrated salt at moderate temperature in atmospheric condition. The material was charge-discharged using lithium salt electrolyte against lithium metal anode instead of potassium since K$^+$ ions are larger in size, a slow diffusion rate into the cathode is expected. So, using lithium as anode, the cation diffusion rate and cell potential also increase because standard reduction potential, E° of Li$^+$ + e$^-$ = Li (-3.04 V) is slightly more negative than that of K$^+$ + e$^-$ = K (-2.93 V).[30]

2. Experimental

2.1 *Material synthesis procedure*

K$_4$Fe(CN)$_6$ was synthesized by heating K$_4$Fe(CN)$_6$.3H$_2$O (BDH, USA, 99%) at 200°C for 4 h in open atmospheric condition. After cooling and grinding, the material was kept out of moisture for further use.

2.2 *Characterization part*

Thermal Gravimetric Analysis (TGA) and Differential Thermal Analysis (DTA) were carried out to find out the heating temperature without decomposition of K$_4$Fe(CN)$_6$.3H$_2$O using a TGA-DTA thermal analyzer (Perkin Elmer, Sweden model number STA 6000) in the temperature region of 40–845°C at a heating rate of 10°C min^{-1}.

The synthesized material was further characterized by using UV-Visible spectroscopy (OPTIZEN POP), Fourier Transform Infrared (FTIR, FTIR-8400S, Shimadzu, Japan), Powder X-ray diffraction (XRD, Ultima III Rigaku Cu Kα, λ =1.5406 Å) and Field Emission Scanning Electron Microscopy (FESEM)-Energy Dispersive X-ray Spectroscopy (EDX) [SUPRA 40 FESEM-EDX, Carl Zeiss SMT AG (Germany)].

The electrochemical characterization of the synthesized material was carried out by cyclic voltametry (CV), chronoamperometry (CA) and charge-discharge studies after preparing a laboratory model cell. The cathode mixture was prepared by mixing the active material (80%) with conducting carbon i.e.; carbon black (Alfa Aesar, USA, 99.9%) (7.5%) with graphite powder (Alfa Aesar, USA, 99.99%) (7.5%); and Polyvinylidene fluoride (Aldrich, USA) (5%) in N-methyl pyrrolidone (NMP) (Merck, USA, 99.5%) as solvent to make homogeneous slurry.[9–12] The slurry, so

obtained, was spread over a thin aluminium foil using a doctor blade to give a uniform distribution over the aluminium surface. NMP, the solvent, was removed by heating the foil coated with the active mixture at 60°C under vacuum. The coated foil was then pressed to achieve a better contact between the active material and the aluminium foil and heated at 80°C for 12 h under vacuum to remove NMP completely. The coated foil was then cooled down to room temperature and thus the positive electrode (cathode) was made ready for cell fabrication.[24]

The cell was assembled inside a glove bag after removing air and moisture completely by purging argon gas. Li (Aldrich, USA, 99.9%) ribbon pasted on a nickel plate was used as anode. One molar LiClO$_4$ (Alfa Aesar, USA, 99%) salt dissolved in (1:1) Ethylene carbonate (Sigma-Aldrich, USA, 98%) and Dimethyl carbonate (Sigma-Aldrich, USA, 99%) mixture and a porous polypropylene (PP) film soaked with this solution were used as electrolyte and separator, respectively.[5–10]

Cyclic voltametry (CV) experiment was carried out using a potentiostat/galvanostat; model VersaStat-II^{TM} (Princeton Applied Research) within the potential window of 1.5 V to 4.5 V vs. Li$^+$/Li at scan rate of 0.5 mVs^{-1} at room temperature. The charge-discharge behaviour of the synthesized material was recorded using the same device in between the potential window of 2.0 V to 4.5 V vs. Li$^+$/Li at the rate of 0.2 C under similar condition. Double potential step chronoamperometry was performed using the same instrument to determine the diffusion coefficients of K$^+$ and Li$^+$ ions applying the step potential of 3.290 and 2.785 V vs. Li$^+$/Li.

3. Result and Discussions

3.1 *Thermal gravimetric analysis (TGA) and differential thermal analysis (DTA)*

TGA-DTA curves, presented in figure 1, show the percentage of mass loss *vs.* temperature of the hydrated salt, K$_4$Fe(CN)$_6$.3H$_2$O. The figure shows that the mass loss occurred at different stages. In the first stage in the temperature range of 40–104°C, a sudden mass loss of 12.4% was observed, which is attributed to the removal of moisture as well as water of crystallisation and the formation of anhydrous K$_4$Fe(CN)$_6$. In the second stage in the temperature range of 104–550°C, a very low (1.2%) or negligible mass loss occurred, which revealed no decomposition in this step. Therefore, it is concluded that anhydrous K$_4$Fe(CN)$_6$ is highly stable up to 550°C. Finally, in the third step,
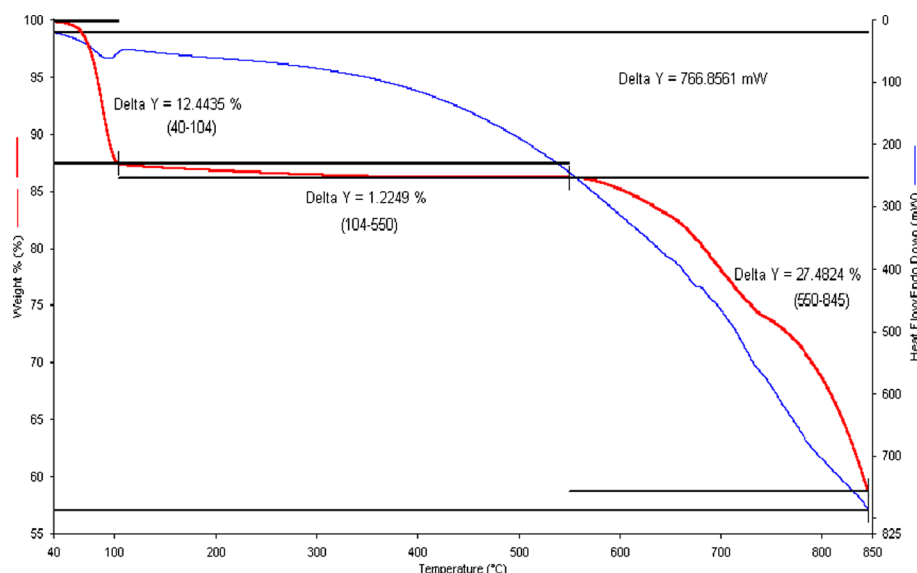
Figure 1. TGA-DTA curve of $K_4Fe(CN)_6.3H_2O$.

decomposition started, and within the temperature region of 550–850°C, 27.5% mass loss was found.

Therefore, from the above study, a moderate temperature of 200°C was chosen for complete dehydration and for crystalline particle growth.

3.2 *UV-Visible spectroscopy*

The UV-Visible spectra of the aqueous solution of hydrated $K_4Fe(CN)_6.3H_2O$ crystal and anhydrous $K_4Fe(CN)_6$ are illustrated in figures 2a and 2b.

A strong absorption at 220 nm, which is the fingerprint of $[Fe(CN)_6]^{4-}$ group, was observed for both the hydrated and anhydrous materials. This reveals

that both the materials contain $[Fe(CN)_6]^{4-}$ group. Furthermore, the anhydrous $K_4Fe(CN)_6$ was prepared from its hydrated salt $K_4Fe(CN)_6.3H_2O$ after heating it at 200°C in open atmosphere, making it vulnerable towards aerial oxidation from $K_4Fe^{II}(CN)_6$ to $K_3Fe^{III}(CN)_6$. But the UV-Visible spectrum negates the formation of ferricyanide due to aereal oxidation, as it is confirmed by comparing with the UV-Vis spectrum (figure 2c) of commercial $K_3Fe(CN)_6$ crystals (BDH, USA, 99%).[31,32] Thus, the material is free from any ferricyanide as impurity. It should be noted that the dehydration of the $K_4Fe(CN)_6.3H_2O$ crystals was required for its use in non-aqueous lithium-ion battery as cathode.

3.3 *FTIR spectroscopy*

FTIR spectrum of dehydrated $K_4Fe(CN)_6$ crystals is shown in figure 3, which shows the strong absorption peaks at 2031 cm^{-1}, 585 cm^{-1} and 424 cm^{-1} attributed to the stretching frequencies of $\nu(CN)$ of $Fe(CN)_6^{4-}$, $\delta(FeCN)$ and $\nu(FeC)$, respectively and they also match well with the literature data.[33−36]

3.4 *Powder x-ray diffraction*

The powder XRD pattern of the anhydrous $K_4Fe(CN)_6$ recorded in the range of $2\theta = 10°–70°$ with scan rate of $5°min^{-1}$ is shown in figure 4. The obtained powder X-ray diffraction pattern was compared with the JCPDS data, file no. 32-0801 and a complete match of peak positions was observed. The analysis shows that the anhydrous $K_4Fe(CN)_6$ has the cell parameters as,
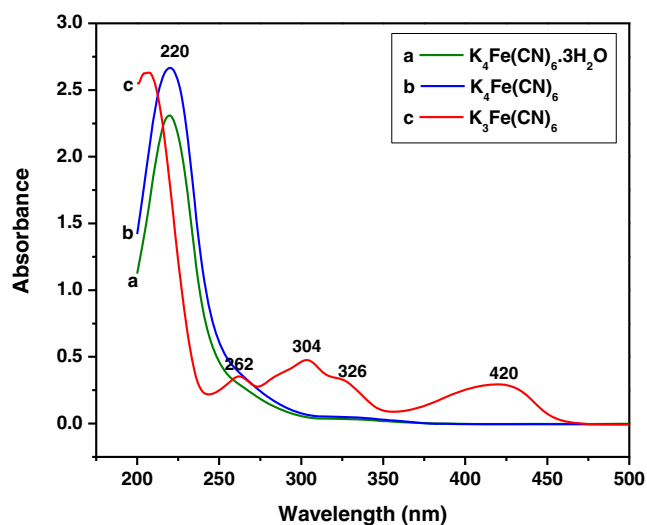
Figure 2. (a) UV-Visible spectra of $K_4Fe(CN)_6.3H_2O$; (b) $K_4Fe(CN)_6$; and (c) $K_3Fe(CN)_6$ in water.

a = 14.02 Å; b = 21.04 Å and c = 4.165 Å, with space group B$_{mmm}$. The sharp peaks indicate the formation of highly crystalline compound with particle size in micron scale.

3.5 *Field emission scanning electron microscopy (FE-SEM)-energy dispersive X-ray spectroscopy (EDX)*

The FESEM images, shown in figure 5, show the surface morphology and the particle size distribution of the hydrated crystals, K$_4$Fe(CN)$_6$.3H$_2$O (figure 5a and 5b), the anhydrous pure materials, K$_4$Fe(CN)$_6$ (figure 5c and 5d) and the materials collected after three cycles of charge-discharge (figure 5e, 5f). The particle size distributions are different in every case. The hydrated material shows the largest particle size distribution with shapes like bricks and sizes varied from 1.8 μ m to 4.0 μ m (figure 5a and 5b). In case of anhydrous K$_4$Fe(CN)$_6$, the particle sizes are relatively smaller and most of their sizes lie within 200 nm to 800 nm range (figure 5c and 5d). The particles are highly ordered and well dispersed; shapes are almost spherical with a few brick-like particles. Very few big size particles are found which resulted from the coagulation of small particles. The small size particles are in good agreement with the cell performance. With decreasing size, the specific surface area of the material increases, which increases the area of host-guest interaction and finally

the capacity retention. Figures 5e and 5f show the surface morphology of the cathode mixture that contained active material, K$_4$Fe(CN)$_6$, carbon black and graphite powder collected after three cycles of charge-discharge. The shapes of the particles and sizes are very similar to those of the starting material. However, a few small size spherical-shaped particles with their sizes in the range of 60–100 nm are found, which might be carbon particles.

The EDX spectra, recorded with the pure anhydrous K$_4$Fe(CN)$_6$ and the active cathode mixture after three cycles of charge-discharge at the rate of 0.05 C are shown in figure 6, spectrum 1 and figure 6, spectrum 2, respectively. The spectral data counting (percentage atomic number) revealed that almost one K$^+$ ion from K$_4$Fe(CN)$_6$ matrix was replaced by one Li$^+$ ion forming of LiK$_3$Fe(CN)$_6$.

3.6 *Electrochemical characterization*

3.6a *Cyclic voltametry*: Figure 7 shows the cyclic voltammograms obtained after sweeping the cathode active material within the potential window of 1.5 V to 4.5 V vs. Li$^+$/Li at the scan rate of 0.5 mV s^{-1}.[27–29]

In the first cycle, an oxidation peak and a reduction peak were observed at 3.91 V and 2.5 V, respectively. But a major shift of the oxidation peak in the negative direction was observed, whereas, the shift of reduction peak was negligible during second cycle. This is because of the removal of heavy K$^+$ ions from the cathode framework which required more energy during the forward scan. Whereas, during reverse scan the vacant sites are occupied by the smaller and highly movable
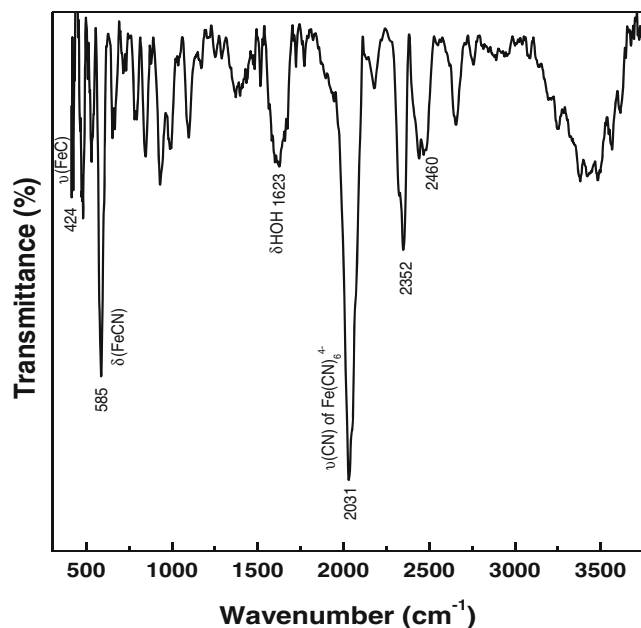
Figure 3. Fourier Transform Infrared (FTIR) spectrum of K$_4$Fe(CN)$_6$.
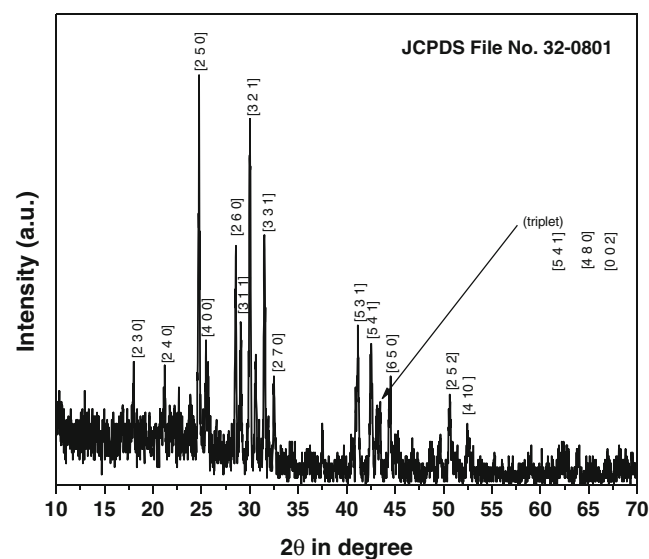
**Figure 4.** Powder X-ray diffraction pattern of anhydrous K$_4$Fe(CN)$_6$.

Li$^+$ ions only. In the subsequent cycles, the oxidation and reduction peak potentials did not alter markedly, as shown in figure 7, but peak current increased upon cycling. The enhancement of peak current is due to the enhancement of ion exchange rate in the cathode material by Li$^+$ than K$^+$ ions.

3.6b *Charge-discharge study*: The typical charge-discharge behaviour of the lab model, coin type cell is shown in figure 8,[27] where the cell was cycled galvanostatically at a rate of 0.2 C rate between the potential window of 2.0 V to 4.5 V vs. Li$^+$/Li. When the cell was charged for the first time, K$^+$ ions were removed from K$_4$Fe(CN)$_6$ matrix. But during discharge process, insertion of cations takes place in a competitive way,

where smaller Li$^+$ ions from electrolytic solution move faster than the larger K$^+$ ion and occupy the vacant sites. Due to the higher mobility and higher exchange rate of Li$^+$ions compared to K$^+$ ions, Li$^+$ will substitute K$^+$ ions in the matrix of the cathode material. Thus, a new composition, Li$_x$K$_y$Fe(CN)$_6$, was obtained from K$_4$Fe(CN)$_6$, where, x + y = 4.

The nature of the charge-discharge curve, illustrated in figure 8, supports this phenomenon. In the first discharge cycle, the cell delivers 32 mAh g^{-1} specific capacity, which gradually increases upon cycling to a maximum value of 61 mAh g^{-1}. The increment can be explained in terms of capacity gain due to removal of Li$^+$ ions at lower potential followed by the removal of K$^+$ ions at higher potential close to 4.5 V vs. Li$^+$/Li. In
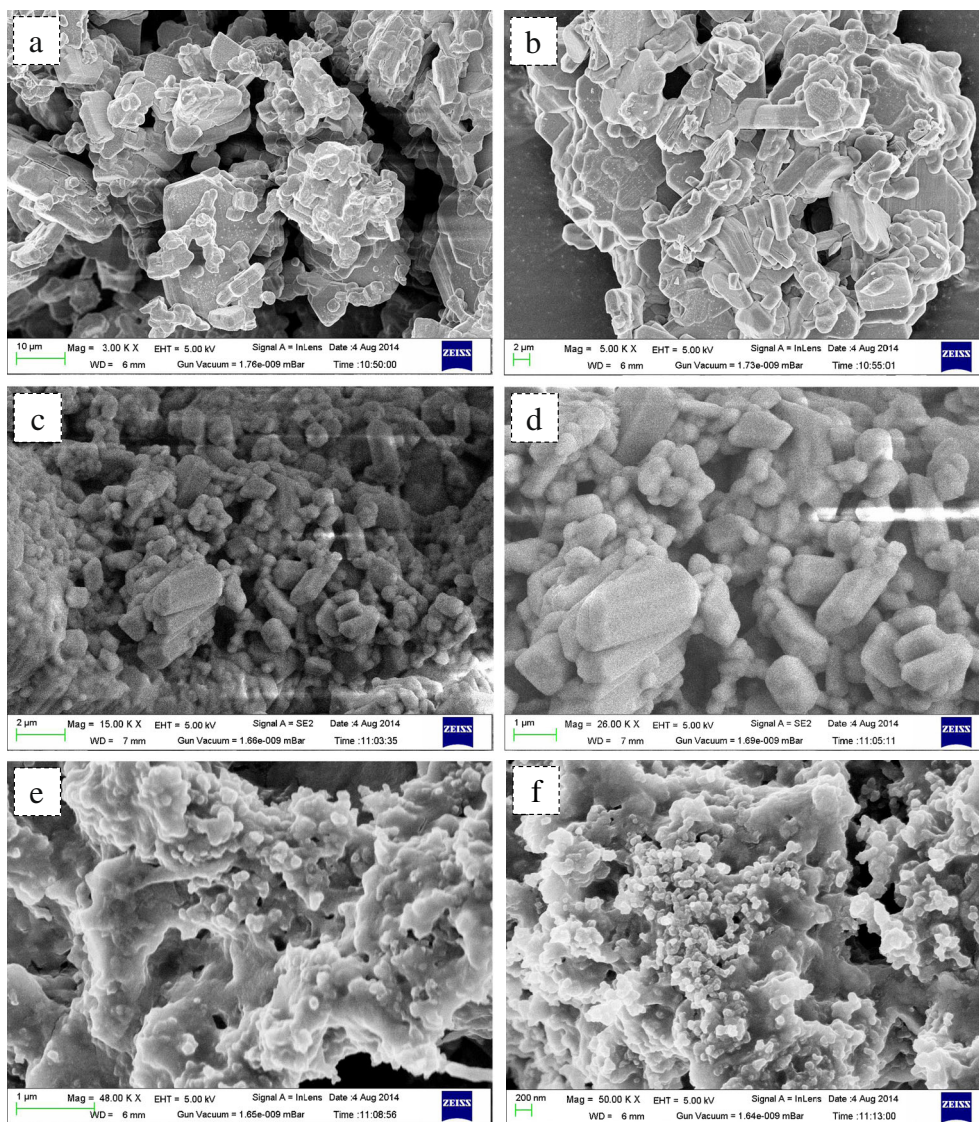

Figure 5. (a, b) FESEM images of K$_4$Fe(CN)$_6$.3H$_2$O; (c, d) anhydrous K$_4$Fe(CN)$_6$ in pure form; (e, f) and cathode mixture prepared with anhydrous K$_4$Fe(CN)$_6$ after three cycles charge-discharge against Li anode.
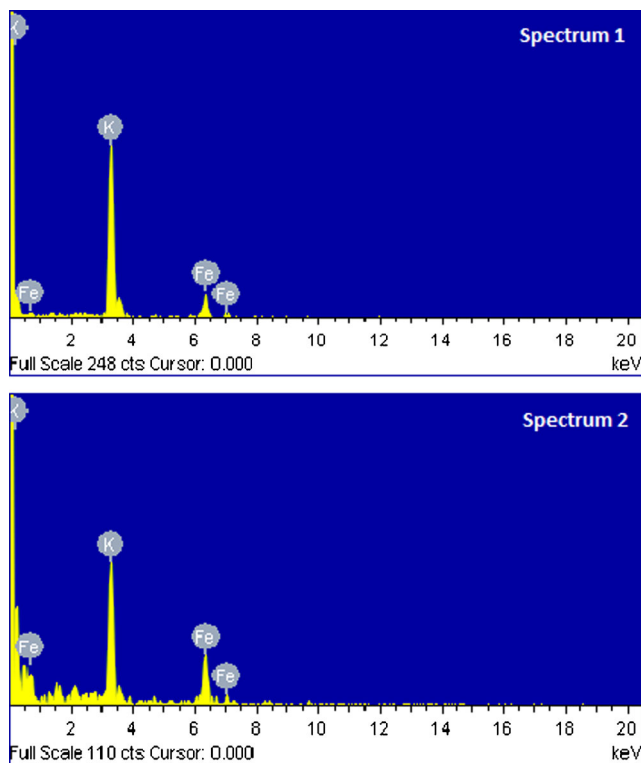
Figure 6. EDX spectra of $K_4Fe(CN)_6$ in pure form (Spectrum 1) and cathode mixture prepared with $K_4Fe(CN)_6$ after three cycles charge-discharge against Li anode (Spectrum 2).

general, discharge capacity of a standard cell decreases upon cycling from the very beginning of the cycling process.[21] But in the present case, the capacity increases very rapidly from the beginning and reaches to a maximum value of 61 mAh g^{-1} which is double of its initial value and 83% of its theoretical specific capacity (72 mAh g^{-1}).
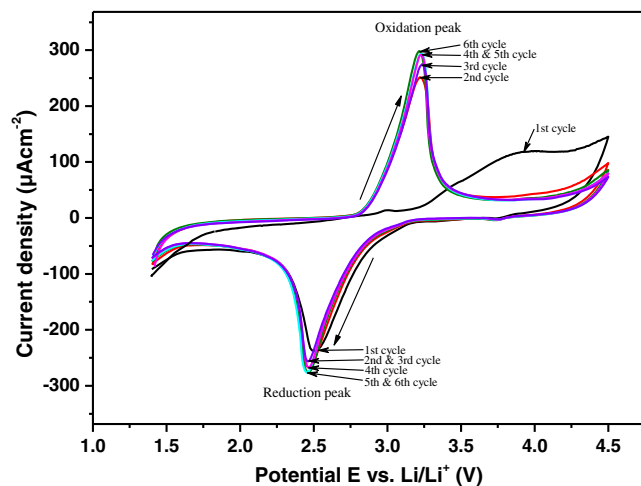
Figure 7. Cyclic voltammogram of anhydrous $K_4Fe(CN)_6$ in 1 Molar LiClO4 solution in EC+DMC (1:1) mixture vs. Li$^+$/Li at the scan rate of 0.5 mVs-1 at room temperature.
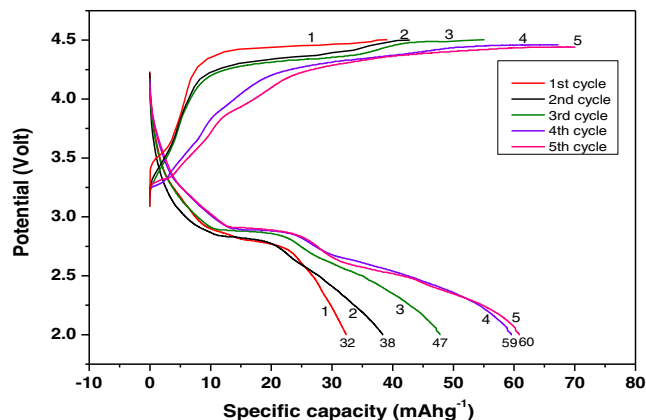

Figure 8. Charge-discharge curves of $K_4Fe(CN)_6$ cathode vs. Li$^+$/Li at rate of 0.2 C at room temperature.

It is interesting to note that during initial charging process, only 50% K$^+$ ions are removed from the $K_4Fe(CN)_6$ matrix due to the restriction of higher limit at 4.5 V to avoid electrolyte decomposition and thus fifty percent of the theoretical capacity is achieved in the initial cycle. But in the subsequent cycles, the capacity gain is observed due to removal of K$^+$ ions at higher potential followed by the removal of newly occupied Li$^+$ ions at lower potential. It should be further noted that when one K$^+$ ion is completely replaced by a Li$^+$ ion forming the composition, $LiK_3Fe(CN)_6$, the cell shows two distinct plateaus, one is at 2.75 V another is at 2.50 V *vs.* Li$^+$/Li and this is explained in terms of phase transition at $Li_{0.5}K_3Fe(CN)_6$ due to removal of fifty percent of the first lithium ion from the $LiK_3Fe(CN)_6$ matrix.

3.6c *Chronoamperometry study*: Chronoamperometry experiment was carried out in order to determine the diffusion co-efficient of Li$^+$ and K$^+$ ions using the following Cottrell equation:

$$i = \frac{nFAD^{1/2}C^b}{(\pi t)^{1/2}} \tag{1}$$

where, n = number of electron(s) transferred per electro-active species; F = Faraday's constant; A = area of the electrode surface in cm^2; D = diffusion coefficient in cm^{2}s^{-1}; C^b = concentration of the electro-active species in mol.cm^{-3}; and t = time in second. In this case, n = 1; F = 96, 486 coulomb mol^{-1}; A = 1.3 cm^2; and C^b = 5.04 x 10^{-3}mol cm^{-3}. It should be mentioned here that C^b was calculated by measuring the density of the solid anhydrous $K_4Fe(CN)_6$ applying relative density measurement technique. The relative density was found 1.8566 g cm^{-3}at 25°C.
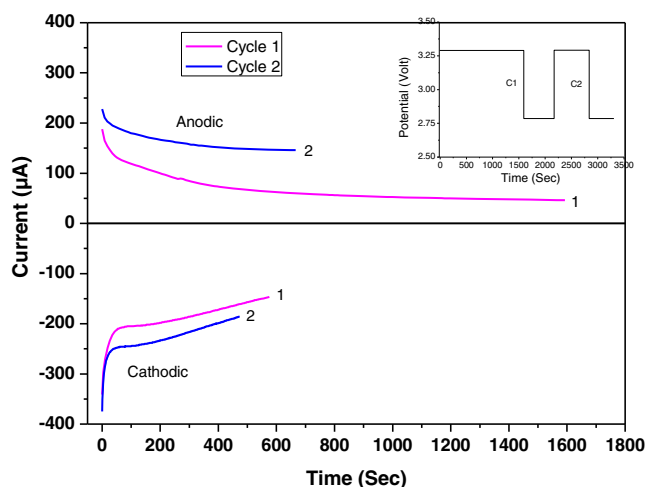
Figure 9. Chronoamperogram of anhydrous $K_4Fe(CN)_6$ in 1 M LiClO$_4$ solution in EC+DMC (1:1) mixture vs. Li$^+$/Li. Inset is potential excitation waveform.

In the chronoamperometry experiment, the potential was stepped from 3.290 V to 2.785 V and the corresponding i-t curve was recorded, as shown in figure 9 (cycle 1). The cell was then charge-discharged galvanostatically at a rate of 0.2 C in order to produce LiK$_3$Fe(CN)$_6$. Using LiK$_3$Fe(CN)$_6$, another set of chronoamperometry experiment was carried out and the corresponding i-t curve was recorded as shown in figure 9 (cycle 2). The diffusion coefficients, obtained after putting the cut off current (i) and time (t) in Cottrell equation, are tabulated in table 1.[37,38] In the first cycle, during anodic scan, K$^+$ ions are removed from K$_4$Fe(CN)$_6$ matrix forming K$_3$Fe(CN)$_6$ and in the reverse cycle, Li$^+$ ions occupy the space vacated by the K$^+$ ions. In the second cycle, only Li$^+$ ions are involved in both the anodic/cathodic process because one K$^+$ ion from K$_4$Fe(CN)$_6$ was replaced by Li$^+$ion forming LiK$_3$Fe(CN)$_6$ during charge-discharge cycles.

The diffusion coefficient calculated from the Cottrell equation, tabulated in table 1, shows that the D$_{K+}$ value of K$^+$ ions is lower than that of Li$^+$ due to its larger size. The diffusion co-efficient (D$_{Li+}$) of the Li$^+$ ions, obtained in the second cycle, are identical as expected, but the value is slightly lower in the first cycle as

Table 1. K$^+$, Li$^+$ ion diffusion coefficients in K$_4$Fe(CN)$_6$ measured in 1 M LiClO$_4$ solution in EC+DMC (1:1) mixture vs. Li$^+$/Li by chronoamperometry using Cottrell equation.

Cycle number	Anodic diffusion coefficient (cm^{2}s^{-1})	Cathodic diffusion coefficient (cm^{2}s^{-1})
1	D$_{K+}$ = 2.68 × 10^{-11}	D$_{Li+}$ = 0.974 × 10^{-10}
2	D$_{Li+}$ = 1.12 × 10^{-10}	D$_{Li+}$ = 1.29 × 10^{-10}

obtained during cathodic sweep. The value, obtained in the first cycle, is lower than expected value, because the concentration of the electro-active lithiated species that has been considered during calculation is 5.04 x 10^{-3} mol.cm^{-3} (C^b), though the actual concentration is low in LiK$_3$Fe(CN)$_6$ in the first cycle.

4. Conclusion

Highly dispersed K$_4$Fe(CN)$_6$ can be synthesized by dehydrating K$_4$Fe(CN)$_6$.3H$_2$O at 200°C in atmospheric condition. The material was used as cathode using lithium salt as electrolyte in a non-aqueous solvent system against lithium metal anode instead potassium. Size of K$^+$ ion being large than Li$^+$, cation diffusion into the cathode material is slow. In order to increase cation diffusion rate capability and ultimately the cell performance, K$^+$ ions were replaced in K$_4$Fe(CN)$_6$ by Li$^+$ ions, by the charge-discharge process. Cyclic voltametry has shown an increasing redox peak current upon cycling, which is explained in terms of faster exchange rate of smaller Li$^+$ ion with larger K$^+$ ion. Similarly, the charge-discharge behaviour of the cathode material at 0.2 C rate has shown an increment in faradic capacity upon cycling, which is explained in terms of the removal of K$^+$ ions at higher potential followed by the removal of Li$^+$ ions at lower potential as cyclic advances are going on. As a result, the capacity increased very rapidly during first few cycles and reached a maximum value of 61 mAh g^{-1} close to its theoretical specific capacity (72 mAh g^{-1}). Furthermore, since the material is non-toxic and cost effective, it may be an economical and environment friendly cathode material for rechargeable Li, K-ion battery.

References

1. Miao C, Bai P, Jiang Q, Sun S and Wang X 2014 *J. Power Sources* **246** 232
2. Patil A, Patil V, Shin D W, Choi J W, Paik D S and Yoon S J 2008 *Mater. Res. Bull.* **43** 1913
3. Fergus J W 2010 *J. Power Sources* **195** 939
4. Sadoway D R and Mayes A M 2002 *MRS Bull.* **27** 590
5. Chen Z, Du B, Xu M, Zhu H, Li L and Wang W 2013 *Electrochim. Acta* **109** 262

6. Wu G, Zhou Y and Shao Z 2013 *Appl. Surf. Sci.* **283** 999

7. Yang X, Xu Y, Zhang H, Huang Y, Jiang Q and Zhao C 2013 *Electrochim. Acta* **114** 259

8. Liu C, Nan J, Zuo X, Xiao X and Shu D 2012 *Int. J. Electrochem. Sci.* **77** 7152

9. Ammundsen B, Desilvestro J, Groutso T, Hassell D, Metson J B, Regan E, Steiner R and Pickering P J 2000 *J. Electrochem. Soc.* **147** 4078

10. Vitins G and West K 1997 *J. Electrochem. Soc.* **144** 2587

11. Su Y, Zou Q, Guo M, Wang Y, Liu J, Yu P and Su J 2004 *J. New Mat. Elect. Syst.* **7** 33

12. Kim D K, Muralidharan P, Lee H W, Ruffo R, Yang Y, Chan C K, Hailin P, Huggins R A and Cui Y 2008 *Nano Lett.* **8** 3948

13. Zhao X, Reddy M V, Liu H, Ramakrishna S, Subba Rao G V and Chowdari B V R 2012 *RSC Adv.* **2** 7462

14. Lee S, Cho Y, Song H K, Lee K T and Cho J 2012 *Angew. Chem.* **51** 8748

15. Padhi A K, Nanjundaswamy K S and Goodenough J B 1997 *J. Electrochem. Soc.* **144** 1188

16. Maccario M, Croguennec L, Cras F and Delmas C 2008 *J. Power Sources* **183** 411

17. Murugan A V, Muraliganth T and Manthiram A 2008 *Electrochem. Commun.* **10** 903

18. Lee S B, Cho S H, Cho S J, Park G J, Park S H and Lee Y S 2008 *Electrochem. Commun.* **10** 1219

19. Beninati S, Damen L and Mastragostino M 2008 *J. Power Sources* **180** 875

20. Jugovic D, Mitric M, Cvjeticanin N, Janèar B, Mentus S and Uskokovic D 2008 *Solid State Ionics.* **179** 415

21. Kim D H and Kim J 2007 *J. Phys. Chem. Solids* **68** 734

22. Mandal B, Basumallick I and Ghosh S 2014 *British J. Appl. Sci Tech.* **4(10)** 1509

23. Wang G X, Bewlay S, Needham S A, Liu H K, Liu R S, Drozd V A, Lee J F and Chen J M 2006 *J. Electrochem. Soc.* **153**(**1**) A25

24. Roberts M R, Spong A D, Vitins G and Owen J R 2007 *J. Electrochem. Soc.* **154** A921

25. Imanishi N, Morikawa T, Kondo J, Yamane R, Takeda Y, Yamamoto O, Sakaebe H and Tabuchi M 1999 *J. Power Sources* **81** 530

26. Imanishi N, Morikawa T, Kondo J, Takeda Y, Yamamoto O, Kinugasa N and Yamagishi T 1999 *J. Power Sources* **79** 215

27. Qian J, Zhou M, Cao Y, Ai X and YangH 2012 *Adv. Energy Mater.* **2** 410

28. Wang X, Hou Y, Zhu Y, Wu Y and Holze R 2013 *Scientific Reports* **3** 1401

29. Ganesh V, Pal S K, Kumar S and Lakshminarayanan V 2006 *J. Colloid. Interface Sci.* **296** 195

30. Lide D R 2005 In *CRC Handbook of Chemistry and Physics* Internet Version (Boca Raton, FL: CRC Press) p 1254

31. Harish S, Joseph J and Phani K L N 2011 *Electrochim. Acta* **56** 5717

32. Chakrabarty M H and Roberts E P L 2008 *J. Chem. Soc. Pak.* **30** 817

33. Klyuev Y A 1965 *J. Appl. Spectrosc.* **3** 30

34. Idemura S, Suzuki E and Ono Y 1989 *Clays Clay Miner.* **37** 553

35. Balmaseda J, Reguera E, Fernández J, Gordillo A and Yee-Madeira H 2003 *J. Phys. Chem. Solids* **64** 685

36. Hussain S, Betsch K and LaCroix C 2003 *IR-Raman Lab*. http://ed.augie.edu/~calacroi/irramanlab.html

37. Jang Y, Neudecker B J and Dudney N J 2001 *Electrochem. Solid-State Lett.* **4**(**6**) A74

38. Park C K, Park S B, Oh S H, Jang H and Cho W 2011 *Bull. Korean Chem. Soc.* **32** 836